Journal Name

COMMUNICATION

Charge transport control via polymer polymorph modulation in ternary organic photovoltaic composites

Received 00th January 20xx,
Accepted 00th January 20xx

DOI: 10.1039/x0xx00000x

www.rsc.org/

Zhipeng Kan [a], Letizia Colella [b, c], Eleonora Canesi [a, b], Alexei Vorobiev [d, e], Vasyl Skrypnychuk [f], Giancarlo Terraneo [a, b], David Barbero [f], Chiara Bertarelli [a, b], Roderick C. I. Mackenzie [g], Panagiotis E. Keivanidis [h]

[a.] *Center for Nano Science and Technology@PoliMi, Istituto Italiano di Tecnologia, Via Giovanni Pascoli, 70/3, 20133 Milano, Italy*
[b.] *Dipartimento di Chimica, Materiali e Ing. Chimica "G. Natta", Politecnico di Milano, piazza Leonardo da Vinci 32, 20133 Milano, Italy*
[c.] *INAF – Osservatorio Astronomico di Brera, via Bianchi 46, 23807, Merate, Italy*
[d.] *Institut Laue-Langevin, 38042 Grenoble Cedex 9, France*
[e.] *Department of Physics & Astronomy, Uppsala University SE-751 20 Uppsala, Sweden*
[f.] *Physics Department, Umeå University, Umeå, Sweden*
[g.] *Faculty of Engineering, University of Nottingham, University Park, Nottingham, UK*
[h.] *Department of Mechanical Engineering and Materials Science and Engineering, Cyprus University of Technology, 45 Kitiou Kyprianou str., 3041 Limassol, Cyprus*

†Electronic Supplementary Information (ESI) available: [2D-GIWAXS data analysis, AFM imaging, SCLC characterization of hole-only devices, TPV characterization of photodiode devices]. See DOI: 10.1039/x0xx00000x

We report a bi-modal distribution observed in the polymer packing distances for ternary solid state composites of the regioregular (rr)-P3HT polymer donor mixed with the PCBM electron acceptor. The formation of two P3HT polymorphs is caused by densely packed and non-densely packed rr-P3HT chains along the lamellar stacking direction. The concentration of the P3HT polymorphs can be selectively tuned when the small molecule of QBT is used as a third component in the blend film. By employing high energy x-ray techniques and opto-electrical characterization techniques we directly link the appearance of the densely-packed P3HT polymorph with an improvement observed in the charge transport property of the ternary P3HT:PCBM:QBT blend films. The formation of the densely-packed P3HT polymorph is specific to the number-averaged molecular weight (M_n) of the rr-P3HT matrix chosen. For the case of a high M_n rr-P3HT batch, negligible amounts of QBT favour the interdigitation of the rr-P3HT side chains and reduce the domain size of the P3HT crystallites, forming the densely-packed P3HT polymorph. Transient photovoltage measurements verify that the fill factor and the short-circuit photocurrent parameters of the P3HT:PCBM:QBT devices are increased the reduced charge carrier recombination rate, when the densely packed P3HT polymorph is present in the photoactive layer.

Solution-processable organic semiconductors based on π-conjugated polymers and small molecules are promising materials for the next generation of light sensing [1] and power-generating semiconductor devices. [2] Low-cost plastic solar cells and photodetectors can be easily fabricated by high throughput wet-deposition techniques. [3] The ability to fabricate devices in this way, combined with potential low cost of organic semiconductor materials, offers the promise of ultra low cost light harvesting devices, e.g. solar cells. The photoactive layer of a typical organic solar cell comprises of a binary system of a π-conjugated polymer blended with small organic molecular acceptor. [4] Light is predominately absorbed in the polymer, which generates a charge neutral exciton with binding energy exceeding that of k_BT. [5, 6] The splitting of the exciton into positive and negative polarons capable of charge conduction, takes place at the donor/acceptor interface. After the exciton has been split, the polarons drift and diffuse to the contacts, facilitated by a network of the donor and acceptor phases in the blend. The overall process of photocurrent generation crucially relies on the microscopic and mesoscopic length scale organization of the donor and acceptor materials. [7] The formation of an optimum microstructure is key in minimizing recombination rates, optimized charge generation rates and maximizing charge carrier mobility. Throughout the deposition of the solution, the solvent rapidly evaporates leaving solidified film on the substrate. During solvent evaporation, both molecular components of the blend tend to reach the lowest free energy configuration giving rise to a non-equilibrium state in which the binary mixture is kinetically trapped. Depending on the glass transition temperature and the chemical structure of the matrix, a distribution of crystalline domains is formed either in the supercooled state of the amorphous polymeric fraction or in the kinetically entrapped glassy state of the composite. The exact balance between the crystalline and the amorphous polymer fractions that are obtained is dictated by kinetic factors, i.e. by the relative magnitude of the rate of crystallization vs the rate of solvent evaporation. [8] Further processing of the composite by post-treatment protocols can modify the structural properties of the layer such as the degree of crystallinity and the size of the crystallites. [9] Many organic materials and their composites exhibit the effect of polymorphism; that is the appearance of multiple crystalline and/or amorphous structural motifs in their solid-state phase, depending on the exact processing and the confinement conditions of the system. [10, 11]

During the last decade several low-temperature and solution-based methodologies have been developed for inexpensively optimizing the structure-property-function correlation in the active layers of organic electronic devices prepared by binary composites. [12] The concentration of the donor/acceptor interfaces can be controlled by varying the composite ratio [13]or the solvent mixture [14]and a fine demixing of the blend components can be achieved in a precise manner via thermal- and/or solvent-vapor annealing steps. [15-18] The control on the nanostructure features of the organic composites enables the accurate tuning of the performance of the corresponding photoactive device. Within this context, further optimization of the device functionalities is achievable when volatile additives are used as morphology modifying agents able to affect the mesoscopic phase separation of the blend components. [19-21] Alternatively, enrichment of the binary blend is possible with a third species that remains in the film after solvent evaporation and that facilitates the enhancement of photocurrent generation through an antenna effect that extents the absorption profile to lower photon energies, that would be otherwise unabsorbed. [22-24] In many cases of ternary organic systems the third component has a multifunctional role that improves the layer morphology, increases the open-circuit voltage and aids light absorption, charge generation and charge transport.[25-29]

Despite the considerable progress in the field of ternary organic semiconductive composites, [28, 30-33] it remains still unclear if the use of a third component can actually affect the occurrence and nature of the polymorph distribution of the polymer matrix in the ternary composite. An obvious example is the case of regioregular poly(3-hexyl-thiophene) (rr-P3HT) which is commonly accepted as the archetypical organic semiconductor in the field of plastic electronics and organic photovoltaic (OPV) devices. [4, 34-36], It has been shown that the overall crystallinity of the rr-P3HT reduces as molecular weight values exceed 12.7 kDa. [37, 38] In the solid state, rr-P3HT forms a lamellar structure in which layers of parallel stacks of polymer backbones are separated by the hexyl side-chains, corresponding to the d_{100} spacing of rr-P3HT crystallites. For single-component P3HT films chain two distinct packing polymorphs can be obtained, which differ in terms of extent of side-chain interdigitation or tilting.; i) a 'dense packing' motif where rr-P3HT layers are densely packed and the lamellar stacking distance is short; [39] and ii) a 'less-dense' packing motif where a larger lamellar stacking distance is observed. [40] To this end the appearance of the two P3HT polymorphs has been observed in single-component rr-P3HT films. [41] Moreover, some indications were presented recently

suggesting the appearance of the densely packed P3HT polymorph in binary blend films of rr-P3HT mixed with [6,6]-phenyl-C_{61} butyric acid methyl ester (PCBM), as provided by grazing-incidence wide angle x-ray scattering (GIWAXS) studies. [42] Nonetheless, it remains unclear whether the formation of the densely-packed P3HT polymorphs correlates with the charge transport properties of the composite and with the performance of the corresponding solar cell device. Addressing this question is of paramount importance for the development of solution-based processing protocols that will be able to deliver next generation organic composites with well correlated structure-property-function relationships.

In this study we demonstrate that the bimodal distribution of the two P3HT polymorphs in P3HT:PCBM blends depends on the number-averaged molecular weight (M_n) of the rr-P3HT batch used and that it can be tuned when a small molecular nucleation agent is employed as a third component in the P3HT:PCBM composite. Interestingly, the formation of the densely packed P3HT polymorph can be triggered when the third component is used in vanishing amounts and it can greatly affect the electrical properties of the corresponding solar cell devices. We show how the bimodal distribution of the two P3HT polymorphs in the binary P3HT:PCBM composite can be precisely tuned with the use of the nucleation agent 5,5′-bis(3,5-di-tert-butyl-4-oxo-2,5-cycloexadien-1-ylidene)-5,5′-dihydro-2,2′-bithiophene (QBT). [43] Ternary P3HT:PCBM:QBT composites are fabricated by keeping the P3HT:PCBM ratio fixed at 1:1 as the QBT content varies between 0 wt% - 3 wt%. The relative content of the P3HT polymorphs is tuned simply by varying the loading of QBT in the ternary system. More importantly, an improvement in the charge transport properties is verified that links directly to the appearance of the densely packed rr-P3HT polymorph, when QBT loadings of 0.3 wt%-0.6 wt% content are used. The chemical structures of the materials studied are shown in Figure 1a. Two sets of P3HT:PCBM:QBT films are investigated, where either a high M_n P3HT (M_n= 65.2 kDa, or a low M_n P3HT (M_n= 36.6 kDa) batch is employed. Care was taken so that the regioregularity of the two rr-P3HT derivatives was the same ($rr_{High\ Mn}$=95.7 % and $rr_{Low\ Mn}$=95.2 %). GIWAXS characterization of films made by the P3HT:PCBM:QBT blends was performed for studying the effect of adding the QBT agent on the relative content of densely packed and non-densely packed P3HT polymorphs. Photodiode devices prepared by the P3HT:PCBM:QBT photoactive layers verify the positive impact on the structural reorganization of the P3HT in the presence of QBT; both photocurrent generation efficiency and charge transport properties are greatly affected when the densely packed polymorph appears in the devices of high M_n rr-P3HT batch. Transient photovoltage (TPV) characterization experiments [44] further inform that the addition of the QBT component results in reduced recombination of charges in the P3HT:PCBM:QBT films, in good agreement with the observed increase in the fill factor (*FF*) parameter of the QBT-containing photodiode devices. For all studied devices the ternary composite layers of P3HT:PCBM:QBT were deposited by spin-coating on glass/ITO/PEDOT:PSS substrates and thermal annealing of these blend films was performed at 140 °C for 15 minutes. Under constant thermal annealing at this temperature, crystallization is kinetically favoured and the crystallization of the blend components starts to evolve. [45]

Figure 1 presents the composition dependent GIWAXS diffraction peaks of the P3HT:PCBM:QBT composites, prepared by the high (Figure 1c) and the low (Figure 1d) M_n rr-P3HT batches. The diffraction intensity monitored is extracted from the corresponding GIWAXS 2D images and it is in the q_Z range between 0.30 $Å^{-1}$-0.56 $Å^{-1}$ that covers the signal corresponding to the d_{100} spacing of rr-P3HT crystallites. [40] From existing single crystal X-ray diffraction data of QBT it is known that QBT reflections are not expected in this q_Z range. [46]Similarly no contribution is expected from the PCBM component which typically appears at higher q_Z values (q_Z ~1.50 $Å^{-1}$). [47, 48] The pertinent parameters (lamellar stacking distances and corresponding domain sizes)of the two P3HT polymorphs in all samples of both high and low M_n samples are reported in Table 1 in correlation to the QBT content used.

Prior to the addition of the QBT component, distinct differences are already observed in the binary P3HT:PCBM composites of high and low M_n samples. Whereas for the high M_n P3HT:PCBM only the type of the no-densely packed P3HT polymorph is found, both densely and no-densely packed P3HT polymorphs can be seen in the low M_n P3HT:PCBM composite. For the high M_n sample (Figure 1c), a single diffraction peak appears, centered at q_z= 0.39 $Å^{-1}$ whereas for the low M_n sample (Figure 1d) the GIWAXS diffraction pattern is a superposition of two peaks centered at q_z= 0.39 $Å^{-1}$ and q_z= 0.41 $Å^{-1}$. These peaks correspond to two different P3HT lamellar stacking distances of 16.2 Å and 14.9 Å, respectively and they are in agreement with previous structural studies of P3HT-only films with similar M_n molecular weights. [41]

The difference in the GIWAXS intensity of the high and low M_n samples suggest that the composite prepared by the low M_n rr-P3HT is more crystalline. This is in a good agreement with specular X-ray diffraction data recorded for the low and high M_n samples (data not shown). Moreover, the difference in the crystallinity of the two systems is further confirmed by atomic force microscopy characterization imaging of these samples (see Supporting Information). [49] Given the comparable regioregularity of both rr-P3HT batches used, we assume that the concentration of the well-ordered domains formed by P3HT chains in the 0 wt% QBT sample primarily depends on the molecular weight of the P3HT matrix. [37, 38] During thermal annealing, the mobility of the shorter P3HT chains is expected to be less confined nucleation sites are formed without the need for external nucleation centers. As such the short P3HT chains crystallize at higher rate leading to a high concentration of small, no-densely packed P3HT crystallites with domain size of 15.2 nm. In contrast, the longer P3HT chains of the high M_n are less mobile and they crystallize at lower rate forming a low concentration of large, no-densely packed P3HT crystallites with a domain size of 17.9 nm. We have previously shown how QBT serves as nucleation agent for the long range organization of the amorphous long polymeric P3HT segments in the P3HT:PCBM:QBT blend. [43] Currently our data verify that the addition of QBT component positively impacts only the composites prepared by high M_n P3HT matrices, most likely via the heterogeneous nucleation of the long P3HT chains.

Strikingly, the addition of QBT in the high M_n ternary composites induces the appearance of the densely packed rr-P3HT polymorph, indicating that the nucleation induced by QBT favors also the formation of P3HT crystallites of shorter lamellar spacing than the typical d_{100} spacing found in P3HT:PCBM blend films. By varying QBT concentration between 0.3 wt% - 3 wt% changes are observed in the relative scattering intensity and the width of the diffraction peaks suggesting that the addition of QBT modulates the bimodal distribution,and the domain size of the two P3HT polymorphs as well as and the overall crystallinity of the ternary P3HT:PCBM:QBT systems. In contrast, the addition of QBT has no effect on the crystallinity of samples of low M_n that are already crystalline due to the low M_n of the rr-P3HT used.

Interestingly, the change in the domain size of the two polymorphs in each set of samples is anti-correlated as the QBT content increases. A reduction is observed in the domain size of the non-densely P3HT polymorph as the domain size of the densely packed P3HT polymorph increases. For both high and low M_n samples, the difference between the size of the two polymorphs is maximized when the QBT content is 0.6 wt% with the non-dense being the largest in size. The magnitude of this difference is the highest for the case of the ternary films of high M_n.

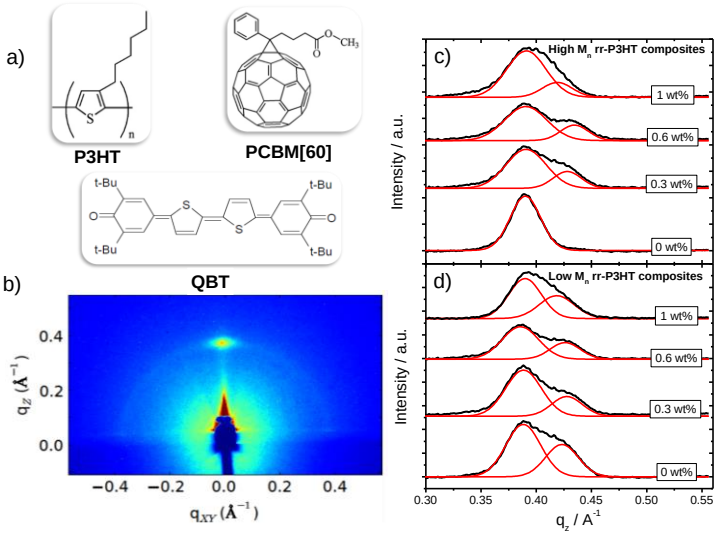

Figure 1. a) The chemical structures of the materials used in this study, b) a representative 2D GIWAXS diffraction pattern registered for the studied P3HT:PCBM:QBT systems, c) QBT-composition dependent GIWAXS diffraction peaks for P3HT:PCBM:QBTcomposite layers of high M_n rr-P3HT, d) QBT-composition dependent GIWAXS diffraction peaks for P3HT:PCBM:QBTcomposite layers of low M_n rr-P3HT. All P3HT:PCBM:QBT layers were of comparable thickness, deposited onto glass/ITO/PEDOT:PSS substrates.

In order to understand the effect of the two co-existing P3HT polymorphs on the electrical properties of the photoactive devices based on the ternary P3HT:PCBM:QBT systems we performed charge transport measurements in unipolar devices (device structure glass/ITO/PEDOT:PSS/P3HT:PCBM:QBT/Au) for deducing the dependence of the zero-field hole mobility of each system on the QBT content. The hole mobility was determined based on the Mott-Gurney equation (see Supporting Information), by taking into account the Poole-Frenkel effect. [27]

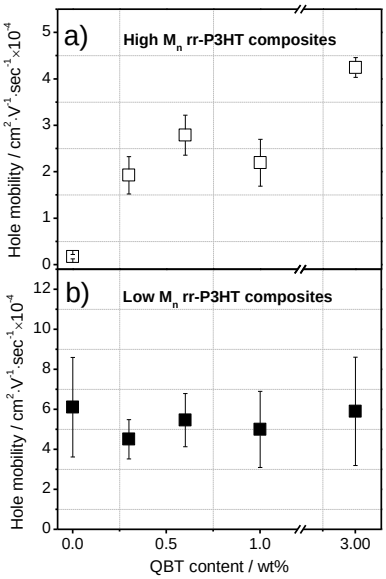

Figure 2. Composition dependent hole mobility of

P3HT:PCBM:QBT blend films prepared by a) a high M_n rr-P3HT batch and b) a low M_n rr-P3HT batch.

Figure 2 presents the QBT composition dependent results of hole mobility values of the studied devices with P3HT:PCBM:QBT photoactive layers prepared by the high M_n rr-P3HT and the low M_n rr-P3HT batches. Given the lower crystallinity of the high M_n samples, it is not surprising that the hole mobility of the corresponding devices is lower than devices of of low M_n. Nonetheless, the addition of a small amount of QBT (i.e. 0.3 wt%) in the P3HT:PCBM:QBT composites of high M_n, leads to an order of magnitude increase when the QBT loading is 0.6 wt%. By increasing the QBT content further the hole mobility also increases, suggesting that the addition of the QBT improves the π-π stacking distance of adjacent P3HT chains. At present we have no structural data available for confirming the QBT-induced optimization of P3HT chain packing along the π-π stacking direction that corresponds to the d_{010} spacing of rr-P3HT crystallites. We can however suggest with caution that the QBT-induced enhancement of the crystallinity along the lamellar stacking direction (d_{100}) could force the P3HT chains in a layer to come closer and to effectively reduce their π-π distance for facilitating charge transport. The recorded GIWAXS patterns of the ternary composites were obtained by scanning the edge-on oriented P3HT fraction of the ternary composites, nonetheless the QBT-induced improvement in the overall crystallinity of the P3HT domains has been previously confirmed by the increase in the enthalpy of melting of the P3HT:PCBM:QBT composites, as provided by thermograms obtained by differential scanning calorimetry experiments. [43] Unlike the case of high M_n devices, the hole mobility in the devices prepared by the low M_n P3HT blends is invariant to the increase of the QBT content suggesting that the addition of QBT induces no severe changes in the π-π stacking distance of adjacent P3HT chains in a layer.

Additional evidence for the direct correlation between the QBT-induced optimization of the layer microstructure and the improvement of device performance is obtained by the composition dependent *FF* parameter of the ternary P3HT:PCBM:QBT photodiodes, following their illumination with simulated solar light (AM1.5G, 0.92 Suns irradiance). Photodiodes were fabricated with P3HT:PCBM:QBT photoactive layers (device structure glass/PEDOT:PSS/P3HT:PCBM:QBT/Al) prepared by the high and the low M_n rr-P3HT batches and by varying the QBT content. Table 2 summarizes the composition dependent main device metrics, obtained from the photo *J-V* curves; that is short circuit photocurrent density (J_{sc}), open-circuit voltage (V_{oc}), *FF* and power conversion efficiency (*PCE*). It can be seen that for the high M_n devices and in respect to the binary P3HT:PCBM system (0 wt% QBT), the *FF* improves by 36% resulting in almost a 50% increase in the *PCE* when QBT is kept at 0.6 wt%. For this QBT content the domain size of the P3HT non-densely packed polymorph undergoes a reduction of 30% and the P3HT densely packed polymorph appears with a domain size of 19.1 nm. In contrast, the use of QBT in devices of low M_n negatively affects all devices metrics with the highest influence observed in the *FF* parameter. In terms of changes in the domain size of the P3HT polymorphs of the low M_n samples, both dense and non-dense P3HT crystallite domains remain unaffected maintaining an average value of 15.2 nm and 16.6 nm, respectively, when the QBT used is in the range of 0 wt%-1 wt%. The ineffective role of QBT in the low M_n ternary composites, underlines the weak influence of QBT in the overall structural properties of P3HT composites with an already optimized crystallinity.

The J_{sc} parameter of devices made by the composites of high M_n material show that despite the continuous increase of hole mobility with increasing the QBT loading, an optimum point is observed for the photocurrent generation. The QBT concentration that corresponds to the optimum J_{sc} is at 0.6 wt% and for higher QBT loadings it is reduced. In the same vein, despite the high hole mobility found for the devices of low M_n material, the addition of QBT negatively influences the photocurrent generation and J_{sc} is gradually reduced as QBT is added in the blend. The gradual deterioration of photocurrent generation, in spite of the improved hole transport properties is attributed to the formation of improper microstructure in the P3HT:PCBM:QBT layers when the QBT content is increased. The addition of high QBT amount (*i.e.* > 0.6 wt%) perturbs the optimized demixing of the P3HT and PCBM phases and it enhances charge recombination as evidenced previously by the reduced concentration of the photogenerated P3HT polarons. [43]

In order to gain a deeper insight on the impact of the structural organization on the electronic properties of the ternary composite systems, we performed transient photovoltage (TPV) measurements to monitor recombination as a function of light intensity. In a TPV experiment, one photoexcites a device at open circuit with a short laser pulse and measures the resulting voltage transient. [50-52] The rate at which the voltage relaxes towards equilibrium conditions can be then used as a measure of charge carrier life time. Interestingly, when processing the TPV data we noted a bi-exponential decay. [44] We attributed the early decay to recombination (photo excited hot carriers recombining with trapped carriers in a Shockley-Read-Hall manner) and the slower longer decay to spatial reorganization of charge carriers in the device/multiple trapping and relaxation events. Figure 3a plots the charge carrier lifetime as a function of QBT content for the P3HT:PCBM:QBT devices prepared by the high M_n rr-P3HT batch. It can be seen that as the QBT content is increased from 0% to 0.6% the carrier life time slows, then as QBT content is further increased carrier life time starts to speed up. This is consistent with the device efficiency data presented above, which shows the 0.6% device to have the highest efficiency. It is also possible that the emergence of the densely packed P3HT polymorph reduces charge recombination, possibly by reducing the number of trap states. [53] If one examines Figure 3b, which plots the charge carrier life time for the P3HT:PCBM:QBT devices prepared by the low M_n rr-P3HT batch as a function of QBT content, it can be seen that the addition of QBT does not affect the recombination life time. This is again consistent with the notion that the binary P3HT:PCBM composite of the low M_n rr-P3HT has already reached an optimum packing configuration and that the addition of QBT has no effect.

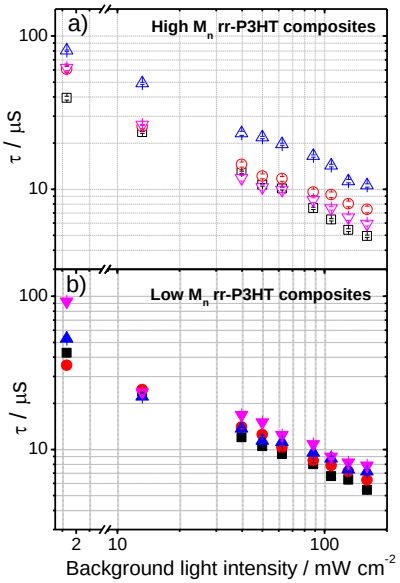

Figure 3. Charge carrier recombination time as a function of background illumination intensity for P3HT:PCBM:QBT devices containing 0 wt% (squares), 0.3 wt% (circles), 0.6 wt% (up-triangles), 1 wt% (down-triangles) prepared by a) a high M_n rr-P3HT batch (open symbols) and b) a low M_n rr-P3HT batch (filled symbols).

Conclusions

In conclusion we have presented a methodology for controlling the distribution of P3HT polymorphs in the ternary composite systems of P3HT:PCBM:QBT. By accurately varying the QBT content in this composite system we induce the formation a densely packed P3HT polymorph that is found to significantly affect the charge transport properties of the P3HT:PCBM:QBT composite layer. The appearance of the densely packed P3HT polymorph is triggered by the QBT component that serves as a nucleation agent. The QBT-induced formation of the P3HT polymorph is specific to the molecular weight of the P3HT matrix used and it is observed in ternary composites based on high M_n P3HT batches. This work suggests that the use of appropriate small organic molecules in ternary systems can modulate the polymorph content in their microstructure via simple solution processing protocols thus offering a valuable tool for tuning the electronic properties of the corresponding organic optoelectronic devices.

The European Synchrotron Radiation Facility (ESRF, Grenoble, France) is acknowledged for providing beam time to beam line BM26. PEK and RCIM are thankful to the Royal Society for a financial support (Travel Grant IE131547).

Notes and references

1. Y. Gao, R. C. I. MacKenzie, Y. Liu, B. Xu, P. H. M. van Loosdrecht and W. Tian, *Adv. Mater. Interfaces*, 2015, **2**.
2. K.-J. Baeg, M. Binda, D. Natali, M. Caironi and Y.-Y. Noh, *Adv. Mater.*, 2013, **25**, 4267–4295.
3. R. R. Søndergaard, M. Hösel and F. C. Krebs, *J. Pol. Sci.: Part B*, 2013, **51**, 16 - 34.
4. M. T. Dang, L. Hirsch and G. Wantz, *Adv Mater*, 2011, **23**, 3597-3602.
5. D. Amarasinghe Vithanage, A. Devižis, V. Abramavičius, Y. Infahsaeng, D. Abramavičius, R. C. I. MacKenzie, P. E. Keivanidis, A. Yartsev, D. Hertel, J. Nelson, V. Sundström and V. Gulbinas, *Nat. Comm.*, 2013, **4**, 1 - 6.
6. S. Gelinas, A. Rao, A. Kumar, S. L. Smith, A. W. Chin, J. Clark, T. S. van der Poll, G. C. Bazan and R. H. Friend, *Science*, 2014, **343**, 512-516.
7. P. E. Keivanidis, T. M. Clarke, S. Lilliu, T. Agostinelli, J. E. Macdonald, J. R. Durrant, D. D. C. Bradley and J. Nelson, *J. Phys. Chem. Lett.*, 2010, **1**, 734–738.
8. J. A. N. Malik, N. D. Treat, M. Abdelsamie, L. Yu, R. Li, D.-M. Smilgies, A. Amassian, C. J. Hawker, M. L. Chabinyc and N. Stingelin, *Org. Photonics Photovolt.*, 2014, **2**, 59–69.
9. S. Malik and A. K. Nandi, *J. Polym. Sci. B*, 2002, **40**, 2073-2085.
10. L. Yu, X. Li, E. Pavlica, F. P. V. Koch, G. Portale, I. da Silva, M. A. Loth, J. E. Anthony, P. Smith, G. Bratina, B. K. C. Kjellander, C. W. M. Bastiaansen, D. J. Broer, G. H. Gelinck and N. Stingelin, *Chem. Mater.*, 2013, **25**, 1823–1828.
11. D. Mon, A. M. Higgins, D. James, M. Hampton, J. E. Macdonald, M. B. Ward, P. Gutfreund, S. Lilliu and J. Rawlef, *Phys.Chem.Chem.Phys.*, 2015, **17**, 2216-2227.
12. R. Shikler, M. Chiesa and R. H. Friend, *Macromolecules*, 2006, **39**, 5393 - 5399.
13. C. Müller, T. A. M. Ferenczi, M. Campoy-Quiles, J. M. Frost, D. D. C. Bradley, P. Smith, N. Stingelin-Stutzmann and J. Nelson, *Adv. Mater.*, 2008, **20**, 3510–3515.
14. F. Zhang, K. G. Jespersen, C. Björström, M. Svensson, M. R. Andersson, V. Sundström, K. Magnusson, E. Moons, A. Yartsev and O. Inganäs, *Adv. Funct. Mater.*, 2006, **16**, 667–674.
15. G. Li, V. Shrotriya, J. Huang, Y. Yao, T. Moriarty, K. Emery and Y. Yang, *Nat. Mater.*, 2005, **4**, 864-868.
16. G. Li, Y. Yao, H. Yang, V. Shrotriya, G. Yang and Y. Yang, *Adv. Funct. Mater.*, 2007, **17**, 1636–1644.
17. Y. Kim, S. A. Choulis, J. Nelson, D. D. C. Bradley, S. Cook and J. R. Durrant, *J. Mater. Sci.*, 2005, 1371-1376.
18. M. Campoy-Quiles, T. Ferenczi, T. Agostinelli, P. G. Etchegoin, Y. Kim, T. D. Anthopoulos, P. N. Stavrinou, D. D. C. Bradley and J. Nelson, *Nat. Mater.*, 2008, **7**, 158-164.
19. J. Peet, J. Y. Kim, N. E. Coates, W. L. Ma, D. Moses, A. J. Heeger and G. C. Bazan, *Nat Mater*, 2007, **6**, 497-500.
20. M.-S. Su, C.-Y. Kuo, M.-C. Yuan, U.-S. Jeng, C.-J. Su and K.-H. Wei, *Adv. Mater.*, 2011, **23**, 3315–3319.
21. S. J. Lou, J. M. Szarko, T. Xu, L. Yu, T. J. Marks and L. X. Chen, *J. Am. Chem. Soc.*, 2011, **133**, 20661–20663.
22. J. Peet, A. B. Tamayo, X.-D. Dang, J. H. Seo and T. Q. Nguyen, *Appl. Phys. Lett.*, 2008, **93**, 163306.
23. M. Koppe, H.-J. Egelhaaf, G. Dennler, M. C. Scharber, C. J. Brabec, P. Schilinsky and C. N. Hoth, *Adv. Funct. Mater.*, 2010, **20**, 338-346.

24. S. S. Sharma, G. D. Sharma and J. A. Mikroyannidis, *Sol Energ Mat Sol C*, 2011, **95**, 1219-1223.
25. M. Campoy-Quiles, Y. Kanai, A. El-Basaty, H. Sakai and H. Murata, *Org Electron*, 2009, **10**, 1120-1132.
26. E. Lim, S. Lee and K. K. Lee, *Chem. Commun.*, 2011, **47**, 914-916.
27. F. Machui, S. Rathgeber, N. Li, T. Ameri and C. J. Brabec, *J. Mater. Chem.*, 2012, **22**, 15570-15577.
28. T. Ameri, P. Khoram, J. Min and C. J. Brabec, *Adv. Mater.*, 2013, **25**, 4245-4266.
29. N. D. Treat, J. A. N. Malik, O. Reid, L. Yu, C. G. Shuttle, G. Rumbles, C. J. Hawker, M. L. Chabinyc, P. Smith and N. Stingelin, *Nat. Mater.*, 2013, **12**, 628 -633.
30. Y. C. Chen, C. Y. Hsu, R. Y. Y. Lin, K. C. Ho and J. T. Lin, *Chemsuschem*, 2013, **6**, 20-35.
31. L. Lu, T. Xu, W. Chen, E. S. Landry and L. Yu, *Nat. Phot.*, 2014, **8**, 716–722.
32. R. A. Street, P. P. Khlyabich, A. E. Rudenko and B. C. Thompson, *J. Phys. Chem. C*, 2014, **118**, 26569−26576.
33. P. P. Khlyabich, A. E. Rudenko, B. C. Thompson and Y.-L. Loo, *Adv. Funct. Mater.*, 2015, DOI: 10.1002/adfm.201502287.
34. P. J. Brown, D. S. Thomas, A. Köhler, J. S. Wilson, J.-K. Kim, C. M. Ramsdale, H. Sirringhaus and R. H. Friend, *Phys. Rev. B*, 2003, **67**, 064203/064201-064203/064216.
35. J. Clark, C. Silva, R. H. Friend and F. C. Spano, *Phys. Rev. Lett.*, 2007, **98**, 206406.
36. M. Brinkmann and P. Rannou, *Adv. Funct. Mater.*, 2007, **17**, 101–108.
37. A. Zen, M. Saphiannikova, D. Neher, J. Grenzer, S. Grigorian, U. Pietsch, U. Asawapirom, S. Janietz, U. Scherf, I. Lieberwirth and G. Wegner, *Macromolecules*, 2006, **39**, 2162-2171.
38. C. Nicolet, D. Deribew, C. Renaud, G. Fleury, C. Brochon, E. Cloutet, L. Vignau, G. Wantz, H. Cramail, M. Geoghegan and G. Hadziioannou, *J. Phys. Chem. B*, 2011, **115**, 12717–12727.
39. S. V. Meille, V. Romita, T. Caronna, A. J. Lovinger, M. Catellain and L. Belobrzeckaja, *Macromolecules*, 1997, **30**, 7898.
40. T. J. Prosa, M. J. Winokur and D. McCullough, *Macromolecules*, 1996, **29**, 3654.
41. S. Joshi, P. Pingel, S. Grigorian, T. Panzner, U. Pietsch, D. Neher, M. Forster and U. Scherf, *Macromolecules*, 2009, **42**, 4651–4660.
42. M. Sanyal, B. Schmidt-Hansberg, M. F. G. Klein, C. Munuera, A. Vorobiev, A. Colsmann, P. Scharfer, U. Lemmer, W. Schabel, H. Dosch and E. Barrena, *Macromolecules*, 2011, **44**, 3795-3800.
43. Z. P. Kan, L. Colella, E. V. Canesi, G. Lerario, R. S. S. Kumar, V. Bonometti, P. R. Mussini, G. Cavallo, G. Terraneo, P. Pattanasattayavong, T. D. Anthopoulos, C. Bertarelli and P. E. Keivanidis, *Sol Energ Mat Sol C*, 2014, **120**, 37-47.
44. R. Singh, E. Aulicio-Sarduy, Z. Kan, T. Ye, R. C. I. MacKenzie and P. E. Keivanidis, *Journal of Materials Chemistry A*, 2014, DOI: 10.1039/C4TA02851A.
45. S. Lilliu, T. Agostinelli, E. Pires, M. Hampton, J. Nelson and J. E. Macdonald, *Macromolecules*, 2011, **44**, 2725–2734.
46. J. Martí-Rujas, unpublished work.
47. E. Verploegen, R. Mondal, C. J. Bettinger, S. Sok, M. F. Toney and Z. Bao, *Adv. Funct. Mater.*, 2010, **20**, 3519–3529.
48. T. Agostinelli, S. Lilliu, J. G. Labram, M. Campoy-Quiles, M. Hampton, E. Pires, J. Rawle, O. Bikondoa, D. D. C. Bradley, T. D. Anthopoulos, J. Nelson and J. E. Macdonald, *Adv. Funct. Mater.*, 2011, **21**, 1701–1708.
49. R. Steyrleuthner, S. Bange and D. Neher, *J. Appl. Phys.*, 2009, **105**, 064509.
50. C. G. Shuttle, B. O'Regan, A. M. Ballantyne, J. Nelson, D. D. C. Bradley, J. de Mello and J. R. Durrant, *Appl. Phys. Lett.*, 2008, **92**, 093311.
51. R. Hamilton, C. G. Shuttle, B. O'Regan, T. C. Hammant, J. Nelson and J. R. Durrant, *J. Phys. Chem. Lett.*, 2010, **1**, 1432–1436.
52. C.-Z. Li, C.-Y. Chang, Y. Zang, H.-X. Ju, C.-C. Chueh, P.-W. Liang, N. Cho, D. S. Ginger and A. K.-Y. Jen, *Adv. Mater.*, 2014, **26**, 6262–6267.
53. R. C. I. MacKenzie, C. G. Shuttle, G. F. Dibb, N. Treat, E. von Hauff, M. J. Robb, C. J. Hawker, M. L. Chabinyc and J. Nelson, *J. Phys. Chem. C*, 2013, **117**, 12407–12414.

Table 1. The lamellar (100) stacking distance (*d*) of the rr-P3HT backbone and the corresponding domain size (*L*) values of the two diffraction peaks found in the GIWAXS patterns of the P3HT:PCBM:QBT composites prepared by the high and the low M_n rr-P3HT batches, as a function of the wt% QBT content. The parameters d_1, L_1 correspond to the non-densely packed rr-P3HT polymorph whereas the parameters d_2, L_2 correspond to the densely packed rr-P3HT polymorph (see text).

P3HT:PCBM:QBT ternary composites of high M_n rr-P3HT batch				
QBT (wt%)	d_1 (Å)	L_1 (nm)	d_2 (Å)	L_2 (nm)
0	16.1	17.9	-	-
0.3	16.1	13.2	14.7	18.8
0.6	16.1	12.6	14.5	19.1
1	16.1	13.5	15.0	17.7
P3HT:PCBM:QBT ternary composites of low M_n rr-P3HT batch				
QBT (wt%)	d_1 (Å)	L_1 (nm)	d_2 (Å)	L_2 (nm)
0	16.2	15.2	14.9	16.3
0.3	16.2	14.8	14.7	17.3
0.6	16.3	14.5	14.8	17.7
1	16.1	16.3	15.0	15.1

Table 2. Summary of hole mobility and performance of P3HT:PCBM:QBT devices with photoactive layers prepared by high M_n rr-P3HTand low M_n rr-P3HT batches, as a function of the wt% QBT content.

QBT content (wt%)		Mobility hole (10^{-4}cm^2 V^{-1} sec^{-1})	V_{oc} (Volts)	J_{sc} (mA/cm^2)	*FF* (%)	*PCE* (%)
High M_n rr-P3HT devices	0	0.17	0.58	6.31	39.8	1.6
	0.3	1.93	0.57	6.69	40.5	1.7
	0.6	2.79	0.57	6.90	54.3	2.3
	1	2.20	0.57	6.24	51.8	2.0
	3	4.24	0.57	5.34	24.2	0.8
Low M_n rr-P3HT devices	0	6.11	0.51	7.5	44.3	1.7
	0.3	4.51	0.44	7.36	37.9	1.2
	0.6	5.46	0.47	6.9	40.3	1.3
	1	5.00	0.51	7.64	38.6	1.5
	3	5.90	0.46	6.83	30.8	1.0

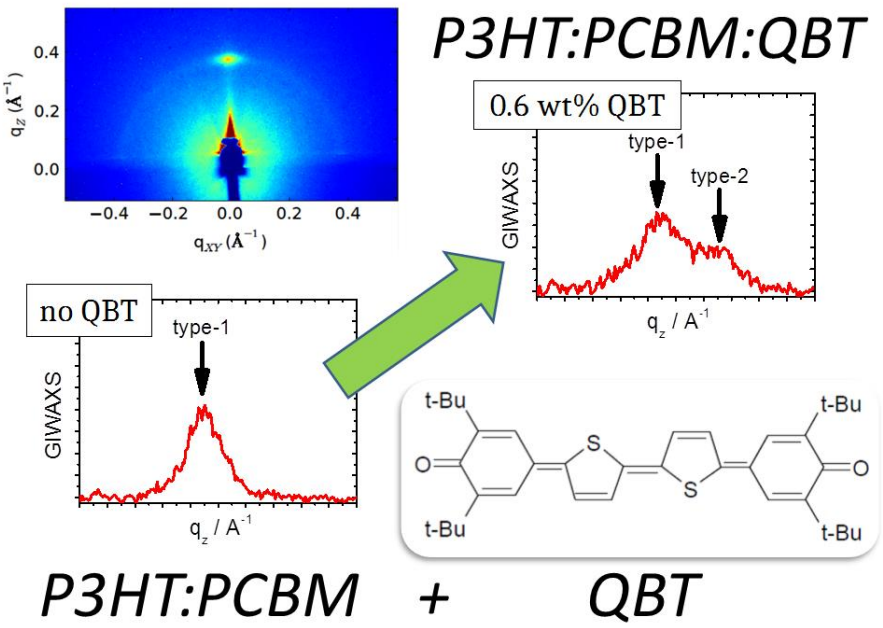
P3HT:PCBM:QBT
0.6 wt% QBT
type-1
type-2
GIWAXS
q_z / A^{-1}
no QBT
type-1
GIWAXS
q_z / A^{-1}
q_z (Å^{-1})
q_{xy} (Å^{-1})
t-Bu
t-Bu
O
S
S
O
t-Bu
t-Bu
P3HT:PCBM + QBT

Journal Name

COMMUNICATION